This is a repository copy of *Multiaxial Fatigue Assessment of Friction Stir Welded Tubular Joints of Al 6082-T6*.

eprints@whiterose.ac.uk
https://eprints.whiterose.ac.uk/

Multiaxial Fatigue Assessment of
Friction Stir Welded Tubular Joints of Al 6082-T6

L. Susmel[1], D. G. Hattingh[2], M. N. James[2,3], R. Tovo[4]

[1]Department of Civil and Structural Engineering, The University of Sheffield, Mapping Street, Sheffield S1 3JD, UK

[2]Department of Mechanical Engineering, Nelson Mandela Metropolitan University, Private Bag X6011, Port Elizabeth 6000, South Africa

[3]School of Marine Science & Engineering, University of Plymouth, Drake Circus, Devon PL4 8AA, England, UK

[4]Department of Engineering, University of Ferrara, via Saragat 1, 44100 Ferrara, Italy

Corresponding Author: Prof. **Luca Susmel**
Department of Civil and Structural Engineering
The University of Sheffield, Mappin Street, Sheffield, S1 3JD, UK
Telephone: +44 (0) 114 222 5073
Fax: +44 (0) 114 222 5700
e-mail: l.susmel@sheffield.ac.uk

Abstract

The present paper addresses the problem of designing aluminium friction stir (FS) welded joints against multiaxial fatigue. After developing a bespoke FS welding technology suitable for joining aluminium tubes, some one hundred welded tubular specimens of Al 6082-T6 were tested under pure axial, pure torsional and biaxial tension-torsion loading. The influence was explored of two independent variables, namely the proportional or non-proportional nature of the biaxial loading and the effect of axial and torsional non-zero mean stresses. The experimental results were re-analysed using the Modified Wöhler Curve Method (MWCM), with this bi-parametrical critical plane approach being applied in terms of nominal stresses, notch stresses, and also the Point Method. The validation exercise carried out using these experimental data demonstrated that the MWCM is applicable to prediction of the fatigue lives for these FS welded joints, with its use resulting in life estimates that fall within the uniaxial and torsional calibration scatter bands. The approach proposed in the present paper offers, for the first time, a complete solution to the problem of designing tubular FS welded joints against multiaxial fatigue loading.

Keywords: friction stir welding, aluminium tubing, multiaxial fatigue, notch fatigue, critical plane

NOMENCLATURE

a, b, α, β	material fatigue constants in the governing equations of the MWCM
k	negative inverse slope
k_0	negative inverse slope of the torsional fatigue curve
$k_\tau(\rho_{eff})$	the modified Wöhler curve's negative inverse slope
B_R	biaxiality ratio ($B_R=\sigma_{x,a}/\tau_{xy,a}$)
F_f	failure force under static axial loading
$K_{t,x}$	gross stress concentration under tension (axial stress)
$K_{t,y}$	gross stress concentration under tension (hoop stress)
$K_{t,xy}$	gross stress concentration under torsion (shear stress)
m	mean stress sensitivity index
N_f	number of cycles to failure
$N_{f,e}$	estimated number of cycles to failure
N_{Ref}	reference number of cycles to failure
Oxyz	system of coordinates
P_S	probability of survival
r_f	fictitious radius
R	load Ratio ($R=\sigma_{x,min}/\sigma_{x,max}$; $R=\tau_{xy,min}/\tau_{xy,max}$)
T_f	failure torque under static torsional loading
T_σ	scatter ratio of the endurance limit for 90% and 10% probabilities of survival
δ	out-of-phase angle
$\Delta\sigma_x$	uniaxial stress range
$\Delta\tau_{xy}$	torsional stress range
σ_1, σ_2, σ_3	principal stresses
σ_n	stress normal to the critical plane
$\sigma_{n,a}$	amplitude of the stress normal to the critical plane
$\sigma_{n,m}$	mean stress normal to the critical plane

$\sigma_x, \sigma_y, \sigma_z$	normal stresses
σ_A	amplitude of the uniaxial endurance limit
ρ_{eff}	critical plane stress ratio
ρ_{lim}	limit value for ρ_{eff}
τ_a	shear stress amplitude relative to the critical plane
τ_A	amplitude of the torsional endurance limit
$\tau_{A,Ref}(\rho_{eff})$	modified Wöhler curve's endurance limit
$\tau_{xy}, \tau_{xz}, \tau_{yz}$	shear stresses

1. Introduction

The impact of fatigue failure on everyday life is evidenced in many high profile and well-publicised structural failures, while highly reputed books on fatigue show that between 50-90% of structural and mechanical assembly problems in service are due to cracking, with fatigue cited as the predominant mechanism [1]. Reviews both in the USA and Europe have indicated that in-service cracking of components costs around 4% of GNP in industrialised nations [2, 3]. Above and beyond the economic cost of fatigue failure, there is often an associated and socially unacceptable cost in terms of loss of human life.

In manufacturing, it is well-known to engineers that one of the most difficult technological issues in fabricating high-performance mechanical assemblies is achieving efficient and reliable joining of the various parts into a structurally sound 'whole'. Welding is the most widely adopted joining solution, even though the overall mechanical performance of welded joints is affected by a number of issues which include, amongst others, flaws induced during welding and the thermal cycle experienced by the material in the weld region. Therefore, the available design standard codes - such as Eurocode 3 [4] and Eurocode 9 [5] - are based on statistically reliable, but very conservative, experimental data linked with a fracture mechanics analysis of crack growth from assumed initial flaws.

Weld quality is a very significant variable which is largely left unspecified in current generation fusion welding codes. In particular, design codes and recommendations set the threshold level for the acceptance of imperfections, whilst fabrication standards give clear indications on the minimum requirements to be met in order to reach an adequate level of safety during in-service operations.

FS joining technology offers a solid-state thermomechanical alternative that provides high weld quality in terms of defect population and a low level of residual stress with relatively high fatigue strength. The high levels of plastic work induced in the weld zone produce dynamically recrystallized fine grains (i.e. in the weld nugget), whilst the low heat input limits distortion and residual stresses to a relatively low fraction of the proof strength of the weld metal. These effects are generally beneficial to weld dynamic performance. Alongside these advantages, the process can also be used to join dissimilar metals and alloys that are difficult to fusion weld. Owing to its specific features, in the recent past this joining technology has been employed successfully in different industrial sectors [6, 7] which include, amongst others: ship building [8], transportation [9], and aircraft [10]. In the case of the aircraft industry both the American Welding Society and NASA have published technical standards for friction stir welding of aerospace components fabricated from aluminium alloys [11, 12].

As far as the fatigue assessment of FS welded joints is concerned, examination of the published state of the art suggests that systematic research work has been carried out since the mid-90s to investigate the fatigue behaviour of FS welded joints in flat plate when they are subjected to uniaxial cyclic loading (see Ref. [13] and references reported therein). In contrast, very little investigation has been so far undertaken on tubular joints or, indeed, on the formulation and validation of specific methodologies suitable for performing multiaxial fatigue assessment of such welds. The major barrier to a wider adoption of tubular aluminium FS welded joints in real structures subjected to in-service time-variable

loading is a lack of suitable multiaxial design procedures underpinned by a systematic knowledge base of experimental, theoretical and analytical work. Hence this paper details the successful development of such a formal methodology for FS welded joints in small diameter aluminium tubes and its validation through suitable experimental data.

2. Fabrication of the FS welded tubular specimens

In order to effectively manufacture the required number of FS welded tubular joints, a bespoke joining technology was developed at the Nelson Mandela Metropolitan University, Port Elizabeth, South Africa, by incorporating a helical SEW worm gear motor with a parent tube clamping system into an MTS I-STIR™ Process Development Platform (Fig. 1a) [14]. This FS welding platform for tubes equipped with a fourth axis was designed and optimised to support the tubes to be joined, to control pin plunge depth and to provide gradual tool retraction so as to eliminate the plunge pin hole. Pin retraction was provided for the MTS i-STIR platform and was accomplished using a hydraulic actuator positioned inside the tool spindle body, with this actuator being coupled with the pin via a threaded adaptor shaft.

As shown in Figs 1a and 1b, the FS welding process involved the SEW helical worm gear motor, the flange coupling, and two bearing supports with integrated clamping devices. The parent material was clamped by sliding two tubes onto a support shaft, with the two tubes being adjusted with precision lock nuts. This sub-assembly system was positioned within the bearing supports by means of Fenlock Cone Clamps (Fig. 1c).

A retractable tool with small diameter shoulder was designed to match the diameter of the thin walled tubes being FS welded (Figs 1c and 1d). Numerous trials were run to determine the influence of the different process parameters on the weld quality and to optimise the tool geometry and pin length. The optimal process variable envelope was required so that an adequate weld surface finish could be achieved. In this respect, the key FS welding

parameters being investigated were: plunge rate, feed rate and spindle rotational speed. The surface finish of the FS welds was further improved by performing two complete revolutions per weld.

The optimal material ligament between tool pin end and supporting shaft was determined by simultaneously considering geometry of the shoulder, pin penetration and parent tube wall thickness. A number of welds were manufactured with variations in these technological parameters and the resulting weld cross sections were assessed in terms of root flaw size and weld consolidation. In particular, it was observed that a better weld consolidation could be obtained by decreasing the shoulder diameter as the smaller surface resulted in a larger effective contact area. A typical weld cross section is shown in Fig. 1e.

Subsequently, the geometry of the FS weld was further optimised by investigating tool tilt angle and shoulder diameter. This second optimisation process gave an optimal tool shoulder undercut by simultaneously defining a tool retraction strategy that resulted in a completely filled and smooth tool stop position. The retraction process occurred over a distance equal to one quarter of the circumference of the tube and eliminated the subsurface tunnel defects that occurred at high retraction rates.

This extensive experimental optimisation led to the following optimal technological parameter envelope: spindle speed=600RPM, plunge depth=2.5mm, pin length=2.45mm, feed rate=50mm/min, tool pitch=2°, and shoulder diameter=10 mm.

These optimised parameters were then employed to manufacture some 120 fatigue specimens that were tested under the following loading conditions: pure axial, pure torsional, and proportional/non-proportional biaxial loading. All tubular samples were made of Al 6082-T6 and had outer nominal diameter equal to about 38 mm and inner nominal diameter to about 31 mm (Figs 2a and 3a). In order to obtain an adequate surface finish, the specimens were FS welded by adopting a double pass strategy (tube rotation of 720°), with the first pass improving the uniformity of the shoulder contact and the second

pass improving the surface finish. The pin penetration depth was initially set to approximately 85% of the nominal tube wall thickness and, as noted above, the quality of the resulting weld was evaluated via metallographic examination. Weld quality was seen to be very sensitive to the alignment of the pin centreline with the joint line. Further, it was observed that the lateral displacement of the pin led to problems associated with weld shoulder undercut and weld ligament variations (potentially resulting in "kissing bonds").

3. Experimental details

Since static strength is a useful indicator of weld quality, the reliability and repeatability of the mechanical properties of the FS welded tubular specimens (Figs 2a and 3) were assessed by carrying out several tensile tests using both complete tubular samples and quasi-flat micro-tensile specimens. Figs 4a and 4b show two examples of static curves generated by testing FS welded tubes under axial and torsional loading, respectively. Owing to the local stress concentration phenomena of the tool undercut on both the advancing and retreating side of the weld (Fig. 2b) failure occurred, as expected, at these grooves (see the pictures in Figs 4a and 4b). At the University of Plymouth, UK, the static strength under axial loading was also measured by testing quasi-flat micro-specimens in a Gatan Microtest 2000EW test stage [14]. This systematic experimental work returned an average value of the axial static strength equal to 303 MPa for the parent material and to 169 MPa for FS welded Al 6082-T6 giving a joint efficiency (defined as the ratio between weld and parent material tensile strength) of 0.55. This value is similar to the values usually reported for thin FS welded plates of 6082-T6 [15]. As to the strength data for the welded 6082-T6 tubes, it is worth observing that the ultimate tensile strength determined by testing quasi-flat micro-specimens was equal to 169 MPa±1.3%, whereas the tensile strength determined by testing FS welded tubes to 168 MPa±1.6%. Even though, as expected, the micro-tensile specimens show a smaller variation in range, the two sets of

data are remarkably consistent, with this confirming the statistical significance of the static results being generated. The average torsional strength was measured to be 118 MPa±1.9%. The fatigue testing trials were run in parallel at the University of Sheffield, UK, and at the University of Ferrara, Italy. The FS welded tubular specimens were tested under uniaxial loading by using an MTS 810 Mod. 318.25 servo-hydraulic machine, the results being generated under load ratios ($R=\sigma_{x,min}/\sigma_{x,max}$) equal to 0.1 and to -1. The force/moment controlled biaxial tests were run under nominal load ratios ($R=\sigma_{x,min}/\sigma_{x,max}=\tau_{xy,min}/\tau_{xy,max}$) equal to 0 and -1 by using a Schenck servo-hydraulic axial/torsional testing machine equipped with two MTS hydraulic grips. The combined axial loading and torsion data were generated under in-phase and 90° out-of-phase constant amplitude sinusoidal load histories.

Tables 1 and 2 summarise the results obtained under R=-1 and R=0÷0.1, respectively, in terms of amplitude and mean value of the nominal stresses in the tube (Fig. 3b), out-of-phase angle, δ, biaxiality ratio, $B_R=\sigma_{x,a}/\tau_{xy,a}$, and number of cycles to failures, N_f. The failure criterion was a 10% stiffness decrease in the tube specimens, with the run-out tests being stopped at $2 \cdot 10^6$ cycles.

The experimental data listed in Tables 1 and 2 were post-processed assuming a log-normal distribution of the number of cycles to failure for each stress level with a confidence level equal to 95% [16]. The results of the statistical reanalysis are summarised in Table 3 in terms of Wöhler curves, where k is the negative inverse slope, σ_A and τ_A are the amplitudes of the axial and torsional endurance limits extrapolated at $N_{Ref}=2 \cdot 10^6$ cycles to failure, and T_σ is the scatter ratio of the amplitude of the endurance limit for 90% and 10% probabilities of survival. Endurance limits σ_A and τ_A reported in Table 3 refer to a probability of survival, P_S, equal to 50%. Table 3 shows that the T_σ ratios obtained for the data generated under pure axial loading as well as under pure torsional loading approach

the unifying value of 1.5 statistically determined by Haibach [17] by post-processing a large number of experimental results obtained under uniaxial fatigue loading from different welded geometries manufactured using standard welding techniques. This further confirms the statistical significance of the results listed in Tables 1 and 2.

The macroscopic cracking behaviour under biaxial loading is summarised in Fig. 5. A detailed investigation of the fracture surfaces [14] revealed that fatigue cracks initiated mainly at the undercut grooves arising from the tool shoulder, on either the advancing or retreating side, (Fig. 2b). In particular, contrary to what had been expected, the weld termination/tool retraction points (see Figure 2a) did not act as "weakest links" in terms of the fatigue strength of the FS welded tubular joints, with about 90% of the specimens failing from cracks initiated at the undercut [14].

Direct inspection of the crack paths revealed that, at a mesoscopic level, initiation and initial propagation occurred mainly on those planes that experienced the maximum shear stress amplitude. This was clearly evident in the specimens tested under torsional cyclic loading where fatigue cracks were seen to initiate and propagate on planes that were either parallel or perpendicular to the longitudinal axis (Fig. 5).

The results reported above suggest that, under fatigue loading, the crack initiation process in these small diameter tubes was primarily governed by the stress concentration phenomena of the weld undercut, with subsequent propagation usually occurring on the material planes that experienced the maximum shear stress amplitude. These two key findings will be used in the following sections of this paper to develop specific design strategies that are suitable for multiaxial fatigue assessment of FS welded tubular joints.

4. Fatigue behaviour under pure axial and pure torsional cyclic loading

Examination of the published literature on the state of the art in fatigue design suggests that, since the mid-1990s, a tremendous experimental effort has been put into

investigating the fatigue behaviour of FS welded plates subjected to uniaxial cyclic loading. In contrast, very little data on fatigue of FS welded tubes have been published in the technical literature so far. Therefore, in the present work, attention was initially focussed on the fatigue behaviour displayed by the tested FS tubular samples under both pure axial and pure torsional cyclic loading.

In the Wöhler diagrams of Figs 6a and 6b, the uniaxial fatigue strength of the FS welded tubes is compared with data for FS welded flat plates. In particular, a systematic bibliographical investigation was carried out to collect fatigue results generated by testing specimens made of 6056-T4, 6061-T6, 6082, 6082-T6 and 6082-T4. These specimens had been manufactured using different combinations of the key welding process parameters [18-31]. The thickness of the FS plate in these data ranged from 0.8-7 mm and the fatigue testing used load ratios of -1, 0, 0.1, 0.2, and 0.5. The reader is referred to the original bibliographical sources for a more detailed description of the various experimental parameters and test methods used in these previous investigations.

According to the numeral system adopted by the International Institute of Welding (IIW) [32], the fatigue strength characterising the data derived from published literature can be accurately modelled using the FAT 28 and the FAT 50 design curves when R≥0 (Fig. 6a) and R=-1 (Fig. 6b), respectively. In the design curves plotted in Figs 6a and 6b, using the recommendations of Sonsino [33] for "thin and flexible" conventional welded joints and of Brasoum [34] for FS welded connections, the negative inverse slope, k, was taken equal to 5.

It is evident in the diagrams of Figs 6a and 6b that, for equivalent values of the stress ratio, the fatigue strength of the FS welded tubes is slightly lower than the corresponding average fatigue strength of the FS welded joints in flat plate. This can be ascribed to the local stress concentration phenomena of the tool shoulder (Fig. 2b). In particular, as noted earlier, direct examination of the crack initiation sites showed that the cracking behaviour of the

tubular joints was primarily governed by the local notch effect associated with the FS welding undercuts [14]. The validity of this experimental conclusion is corroborated by the fact that, in general, undercut grooves (both on the advancing and on the retreating side of the weld) are seen to be much less pronounced [35-41] in joints made in flat plate than they are in joints made in small diameter tubes; this would result in lower values for the associated stress concentration factors in flat plate specimens.

Turning to a consideration of the mean stress effect, Figure 6c suggests that the fatigue strength of the FS welded tubes is strongly affected by the presence of a superimposed mean stress, with this holding true even though the specimens were tested in the as-welded condition. This is believed to be due to the lower levels of residual stress induced during the solid-state FS process which makes FS welded connections more sensitive to the presence of non-zero mean stresses. According to Table 3, the endurance limit (at $2 \cdot 10^6$ cycles to failure) under uniaxial fatigue loading ($B_R=\infty$) is seen to decrease from 33.5 MPa at R=-1 to 18.6 MPa at R=0.1, with the negative inverse slope decreasing from 6.5 to 4.4.

The Wöhler diagram of Fig. 6d plots, in terms of nominal shear stress amplitude, $\tau_{xy,a}$, the experimental data obtained with a torsional load ratio, R, equal to -1 and 0, and the corresponding results from the statistical reanalysis are given in Table 3 ($B_R=0$).

The torsional endurance limits, τ_A, reported in Table 3 indicate that non-zero superimposed mean shear stresses in the fatigue cycle had little effect on the torsional fatigue strength of these FS welded tubes, with τ_A at $2 \cdot 10^6$ cycles to failure decreasing from 38.9 MPa at R=-1 to 32.9 MPa at R=0. This experimental evidence again agrees with observations made in un-welded metallic materials where the presence of superimposed static torsional stresses can be disregarded with little loss of accuracy in fatigue life estimation, provided that the maximum shear stress in the cycle is lower than the material shear yield stress [42, 43]. Figure 6d shows the results of the statistical reanalysis obtained by grouping together the experimental data generated in these FS welded tubes at both

R=-1 and R=0; the relatively low value obtained for index T_σ confirms that the torsional fatigue strength of the FS welded tubular joints is only marginally affected by the presence of non-zero mean shear stresses.

Turning back to the statistical reanalysis summarised in Table 3 for $B_R=0$, the values of the negative inverse slope, k, are seen to be larger than the value of 5 recommended by the IIW to assess the torsional fatigue strength of conventional aluminium welded joints [32]. The k values for $B_R=0$ listed in Table 3 are also larger than the unifying value of 7 suggested by Sonsino at al. [33] for use in designing conventional aluminium welded joints that can be classified as "thin and flexible" under torsional fatigue loading. This indicates that the local stress concentration phenomena due to the undercut grooves (Fig. 2b) has a less pronounced effect under cyclic torsion than under uniaxial fatigue loading (see Figures 6a and 6b). This results in negative inverse slopes under torsional fatigue loading that approach the k values usually displayed by un-welded aluminium alloys [44].

Together with the observed cracking behaviour [14], the considerations reported above suggest that the fatigue strength of these FS welded tubes was largely affected by the stress concentration associated with the undercut grooves (Fig. 2b). Therefore, it can be postulated that the fatigue assessment of these small diameter tubular joints can be performed accurately by simply treating the design issue as a conventional notch fatigue problem. Furthermore, if the stress concentration phenomena are assumed to be more influential than the effect of the joining technology, the fatigue behaviour of the FS welded tubes under both uniaxial and torsional fatigue loading should be amenable to being modelled via the notch stress concept [44, 45] together with those design curves that are recommended for conventional welded joints [46].

The diagrams reported in Figs 6e and 6f summarise the results obtained by rounding the undercut grooves with a fictitious root radius equal to 0.05 mm. Notch stresses were determined, both under uniaxial (Fig. 6e) and torsional fatigue loading (Fig. 6f), from

linear-elastic axi-symmetric bi-dimensional Finite Element (FE) models solved using commercial software ANSYS®. In order to perform the stress analysis accurately, the mesh density in the vicinity of the undercut was gradually increased until convergence occurred. This resulted in an element size in the highly stressed regions of the order of 0.001 mm. Since the wall-thickness of the parent tube was lower than 5 mm, these FE models invariably assumed the fictitious radius, r_f, to be equal to 0.05 mm, as recommended by Sonsino [46]. This numerical stress analysis gave gross stress concentration factors of $K_{t,x}$=4.44 and $K_{t,y}$=1.16 under tension, and $K_{t,xy}$=2.48 under torsion.

The Wöhler diagram shown in Fig. 6e shows that the FAT 160 design curve with inverse slope, k, equal to 5 (as recommended by Sonsino [33, 46] to be used to perform the fatigue assessment of "thin and flexible" conventional welded joints) is capable of accurately modelling the uniaxial fatigue behaviour of these nominal 38 mm diameter FS welded tubes for both R=-1 and R=0. Similarly, the Wöhler diagram in Fig. 6f clearly shows that the FAT 90 design curve with k=7 [33, 46] is suitable for performing the fatigue assessment for these FS welded aluminium tubes in cyclic torsion, giving slightly conservative estimates of fatigue life.

In summary, for these FS welded tubes of 6082-T6, the observations reported in this paper allow the following conclusions to be drawn:

1) under uniaxial cyclic loading, the overall fatigue strength is influenced by the presence of non-zero mean stresses (Fig. 6c);

2) under torsional fatigue loading, the presence of superimposed static shear stresses can be neglected with little loss of accuracy (Fig. 6d);

3) the crack initiation phenomenon is governed by the stress concentration phenomena due to the undercut grooves arising from the tool shoulder (Fig. 2a) [14];

4) fatigue assessment can be performed using standard notch fatigue concepts (Figs 6e and 6f).

These outcomes will be used in the following section to formulate a specific methodology suitable for designing small diameter aluminium FS welded tubular joints against multiaxial fatigue loading.

5. Fundamentals of the MWCM

The formulation of the so-called Modified Wöhler Curve Method (MWCM) is based on the assumption that fatigue damage reaches its maximum value on the material plane that experiences the maximum shear stress amplitude (i.e., the so-called critical plane). Since, as discussed above, in these FS welded joints the fatigue crack initiation process was seen to be mainly shear stress dominated (at least, at a mesoscopic level), the MWCM was taken as a starting point to devise specific design procedures suitable for multiaxial fatigue assessment of FS welded tubes. In the following discussion, the key features of the MWCM will be reviewed briefly by addressing the problem in its most general form. Subsequently, the accuracy of the design methodology being proposed will be checked against the experimental results summarised in Tables 1 and 2 by applying the MWCM in terms of nominal stresses, notch stresses, and also the Point Method.

Independently from the degree of multiaxiality of the applied loading path, the MWCM quantifies the extent of fatigue damage using the stress components relative to the critical plane. In more detail, the combined effect of the shear and normal stresses acting on the material plane that experiences the maximum shear stress amplitude, τ_a, is assessed via the following effective stress ratio [44, 47, 48]:

$$\rho_{eff} = \frac{m \cdot \sigma_{n,m} + \sigma_{n,a}}{\tau_a} \tag{1}$$

where $\sigma_{n,m}$ and $\sigma_{n,a}$ are, respectively, the mean value and the amplitude of the stress perpendicular to the critical plane. Mean stress sensitivity index m is a material fatigue property whose value ranges from zero (no mean stress sensitivity) to unity (full mean

14

stress sensitivity) and that must be determined experimentally [49]. From a stress analysis viewpoint, the ratio ρ_{eff} is seen to be sensitive to the presence of non-zero mean stresses as well as to the degree of multiaxiality and non-proportionality of the load history being assessed [44, 49]. In particular, ρ_{eff} is equal to unity under fully-reversed uniaxial fatigue loading, whereas it is invariably equal to zero under cyclic torsion [44, 47].

In order to understand the *modus operandi* of the MWCM, consider the modified Wöhler diagram sketched in Fig. 7a on log-log axes which plots the shear stress amplitude relative to the critical plane, τ_a, against the number of cycles to failure, N_f. In this diagram, the fatigue strength of the material and component being designed can be estimated through different modified Wöhler curves whose position changes as the ratio ρ_{eff} varies. In the most general scenario, these curves are characterised by different values of both the negative inverse slope, $k_\tau(\rho_{eff})$, and the endurance limit, $\tau_{A,Ref}(\rho_{eff})$, extrapolated at N_{Ref} cycles to failure (Fig. 7a).

As suggested by the schematic diagram shown in Fig. 7a, fatigue lifetime can directly be estimated via the shear stress amplitude relative to the critical plane, τ_a, provided that the necessary design curve is available for the specific value of the ρ_{eff} ratio under investigation. Noting that, in situations of practical interest, the experimental fatigue curves that are usually available to structural designers are those generated under fully-reversed uniaxial (ρ_{eff}=1) and torsional (ρ_{eff}=0) fatigue loading, any other modified Wöhler curve must be estimated. By performing a systematic investigation involving a large number of experimental results, it has been demonstrated that accurate predictions can be made by using simple linear laws to define the relationships $k_\tau(\rho_{eff})$ and $\tau_{A,Ref}(\rho_{eff})$ [44, 47, 48], i.e.:

$$k_\tau(\rho_{eff}) = \alpha \cdot \rho_{eff} + \beta \tag{2}$$

$$\tau_{A,Ref}(\rho_{eff}) = a \cdot \rho_{eff} + b \qquad (3)$$

In Eqs (2) and (3) α, β, a and b are material fatigue constants that should be determined by running appropriate experiments [44]. If the constants in the MWCM are calibrated using fatigue curves generated under fully-reversed uniaxial ($\rho_{eff}=1$) and torsional ($\rho_{eff}=0$) cyclic loading, relationships (2) and (3) can be rewritten as follows [44]:

$$k_\tau(\rho_{eff}) = [k - k_o] \cdot \rho_{eff} + k_o \qquad (4)$$

$$\tau_{A,Ref}(\rho_{eff}) = \left(\frac{\sigma_A}{2} - \tau_A\right) \cdot \rho_{eff} + \tau_A \qquad (5)$$

In Eq. (4) k and k_o are used to denote the negative inverse slope of the uniaxial and torsional fatigue curves, respectively, whereas σ_A and τ_A in Eq. (5) are the amplitudes of the corresponding endurance limits at N_{Ref} cycles to failure (Fig. 7a).

It is important to point out here that relationships (4) and (5) can be used to estimate the position of the necessary modified Wöhler curve as long as the ratio ρ_{eff} is lower than a specific threshold value (denoted as ρ_{lim}) which must also be determined experimentally [44]. As shown in Fig. 7b, for $\rho_{eff} > \rho_{lim}$, both $k_\tau(\rho_{eff})$ and $\tau_{A,Ref}(\rho_{eff})$ are recommended to be taken as constant and equal to $k_\tau(\rho_{lim})$ and $\tau_{A,Ref}(\rho_{lim})$, respectively [44]. This correction was introduced to model (in an engineering way) the fact that, under high values of ratio ρ_{eff}, fatigue damage is no longer primarily shear stress dominated. Under these circumstances, the use of the classic critical plane approach provides life estimates that are characterised by an excessive degree of conservatism [49, 50]. This can be ascribed to the fact that when $\sigma_{n,m}$ exceeds a certain material-dependant threshold value, a further increase in the mean normal stress does not result in a further increase in the associated

fatigue damage [49, 51]. This can be explained by observing that, as $\sigma_{n,m}$ is lower than the above material threshold, the magnitude of the shearing forces driving the propagation process is reduced due to the friction between the crack surfaces. This leads to an inevitable reduction in the crack growth rate. In contrast, as micro/meso cracks are open, the shearing forces are fully transmitted to the tips of such cracks, with this favouring a Mode II propagation. Therefore, once a crack is fully open, a further increase of $\sigma_{n,m}$ does not result in an increase in the associated crack growth rate [51]. According to this damage model, the corrections for the relationships $k_\tau(\rho_{lim})$ and $\tau_{A,Ref}(\rho_{lim})$, which are briefly recalled above (see Fig. 7b), allow the contribution of the stress perpendicular to the critical plane to be taken into account in a more accurate way [44].

Turning back to the *modus operandi* of the MWCM, once Eqs (4) and (5) have been used to obtain the modified Wöhler curve for the specific value of the ρ_{eff} ratio being investigated, the number of cycles to failure can be estimated by using the following standard Wöhler-type equation (Fig. 7a):

$$N_{f,e} = N_{Ref} \cdot \left[\frac{\tau_{A,Ref}(\rho_{eff})}{\tau_a} \right]^{k_\tau(\rho_{eff})} \tag{6}$$

The most critical task in using the MWCM to obtain accurate life estimates is the correct determination of the stress components relative to the critical plane. Current service experience suggests that the highest level of accuracy is obtained by calculating τ_a, $\sigma_{n,m}$, and $\sigma_{n,a}$ using the so-called Maximum Variance Method [52, 53, 54].

It is worth observing here that the MWCM can be applied also by adopting other definitions to calculate τ_a - such as, for instance, the Minimum Circumscribed Circle concept devised by Papadopoulos (see Refs [44, 52] and the references reported therein for a detailed review of the available definitions suitable for calculating the shear stress amplitude relative to the critical plane). The advantage of the Maximum Variance Method over the other existing definitions is that, thanks to its *modus operandi* [52], it is no longer

necessary to project the load history on a given set of material planes in order to determine the critical one. This is due to the fact that, unlike the classic definitions, the stress analysis is performed by the Maximum Variance Method in terms of variance of the resolved shear stress and not in terms of shear stress acting on a given plane. This strategy results also in remarkable computational efficiency. In fact, as soon as the variance and covariance terms relative to the input load history being investigated are known, the time required to calculate τ_a does not depend on the length of the assessed load history [52].

Turning back to the MWCM, it is worth observing here also that this design criterion has been found to provide accurate estimates of the multiaxial fatigue life of conventional steel or aluminium welded joints [55, 56]. In particular, accurate predictions can be made by applying the MWCM not only in terms of nominal [57-60] or hot-spot stresses [55, 56, 59, 61], but also using the reference radius concept [59, 62] or the Theory of Critical Distances [59, 63-65].

Independently of the stress analysis strategy being adopted, the MWCM is seen to be capable of estimating the fatigue strength of welded joints not only when they work in the as-welded condition, but also when they are stress-relieved [56, 62-64].

Much experimental evidence suggests that in as-welded joints subjected to cyclic loading the presence of superimposed static stresses can be neglected with little loss of accuracy. This is due the effect of the residual stresses arising from the welding process. In particular, under fatigue loading, high tensile residual stresses alter the actual value of the load ratio in the weld region, so that, the local value of R becomes larger than zero even when the nominal load ratio approaches -1. Accordingly, connections in the as-welded condition can be designed accurately by simply adopting reference fatigue curves generated under R ratios larger than zero. The detrimental effect of residual stresses can be mitigated by relieving the welded material via appropriate technological processes. By so

doing, the fatigue strength of weldments increases, but, at the same time, they become more sensitive to the presence of non-zero mean stresses.

In this context, as the MWCM is applied in terms of either nominal stresses, hot-spot stresses, or the reference radius concept, the presence of residual stresses can be taken into account directly by simply multiplying the reference endurance limit of the modified Wöhler curve being adopted by a suitable enhancement factor [56, 62]. In contrast, when the MWCM is used along with the Theory of Critical Distances, as recommended by Eurocode 3 [4], the beneficial effect of residual stresses is modelled via an effective shear stress range that is calculated by adding the tensile part to 60% of the compressive part of the loading cycle [63, 64].

To conclude, it can be observed that, since the FS welded specimens sketched in Figure 3 were tested in the as-welded condition, in what follows the fatigue curves generated under both uniaxial and torsional fully-reversed loading will be used to calibrate the MWCM directly. However, according to the strategies briefly mentioned above, this critical plane approach is expected to be successful in designing also stress-relieved FS welded joints provided that the calibration fatigues curves are corrected via appropriate enhancement factors.

6. Accuracy of the MWCM in designing FS welded joints against multiaxial fatigue

In order to evaluate the reliability of the MWCM in performing a multiaxial fatigue assessment for small diameter FS welded tubular joints, the accuracy of this approach can be checked against the experimental results listed in Tables 1 and 2. This validation exercise will use several strategies to determine the relevant time-variable stress states. In particular, the MWCM will applied in terms of both nominal and notch stresses as well as via the Theory of Critical Distances used in the form of the Point Method (PM).

6.1. Stress/strength analysis strategies

To apply the MWCM in terms of nominal stress, the linear-elastic stress components at the critical locations were calculated according to classical continuum mechanics, using the nominal gross area as the reference cross-section (see Fig. 3b).

The required notch stresses and the relevant stress fields in the vicinity of the weld undercut (Figs 2b and 3c) were determined by solving axisymmetric bi-dimensional linear-elastic FE models using commercial software ANSYS®. As noted earlier in the paper, in the vicinity of the tool shoulder grooves the mesh density was gradually increased until convergence of the model occurred, this process resulting in elements having, in the process zone, a size of the order of 0.001 mm. To post-process the results generated under biaxial loading, the relevant linear-elastic stress states/fields were initially calculated numerically under pure axial and pure torsional loading, with the total stress states/fields being subsequently determined using the superposition principle [44].

Finally, independently from the stress analysis strategy being adopted, fatigue strength was estimated according to the MWCM applied through our own software Multi-FEAST© (www.multi-feast.com).

6.2. MWCM and nominal stresses

To apply the MWCM in terms of nominal stresses, the calibration constants in Eqs (2) and (3) were estimated according to Eqs (4) and (5) using the parameters reported in Table 3 that characterise the fully-reversed uniaxial ($B_R=\infty$) and fully-reversed torsional ($B_R=0$) fatigue curves. The diagram in Fig. 8a presents the calibration results plotted in terms of modified Wöhler curves, with the corresponding stress quantities relative to the critical plane being shown in Fig. 8b using Mohr's circles. The results summarised in Fig. 8a allow the MWCM's governing equations to be calibrated directly, giving:

$$k_\tau\left(\rho_{eff}\right)=-4.3\cdot\rho_{eff}+10.8 \tag{7}$$

$$\tau_{Ref}\left(\rho_{eff}\right)=-22.2\cdot\rho_{eff}+38.9 \ \text{MPa} \tag{8}$$

As mentioned earlier, the fatigue strength of these FS welded joints in tensile loading was seen to be highly sensitive to presence of non-zero mean axial stresses (Fig. 6c), even though the specimens were tested in the as-welded condition. The mean stress sensitivity was quantified via the R=0.1 uniaxial fatigue curve obtaining: m=1 and ρ_{lim}=1.3.

The experimental data for cycles to failure, N_f, versus the estimated number of cycles to failure, $N_{f,e}$, is shown in Fig. 9a and demonstrates that the MWCM applied in terms of nominal stresses gives accurate life estimates, that fall within the wider scatter band associated with the two modified Wöhler curves (Fig. 8a) that were used to estimate the constants in the MWCM's governing equations.

6.3. MWCM and notch stresses

Owing to the stress concentration associated with the undercut grooves, the MWCM was used to post-process the results summarised in Tables 1 and 2 by also applying it in terms of notch stresses [45, 59, 62]. Systematic measurements made both on the retreating and the advancing sides of the welds resulted in an average value for the undercut root radius approaching 0.5 mm (Fig. 2b). The corresponding gross stress concentration factors were determined numerically, giving $K_{t,x}$=2.4 and $K_{t,y}$=0.48 under tension, and $K_{t,xy}$=1.7 under torsion.

The uniaxial and torsional fully-reversed fatigue curves post-processed in terms of notch stresses were then used to estimate the constants in Eqs (2) and (3). For the sake of clarity, these two curves (together with the associated experimental results) are plotted in Fig. 8c in terms of linear-elastic stresses at the undercut tip (Fig. 3d), the corresponding stress

components relative to the critical plane being shown in Fig. 8d. This calibration process gave the following values for the constants in the MWCM's governing equations:

$$k_\tau(\rho_{eff}) = -4.3 \cdot \rho_{eff} + 10.8 \qquad (9)$$

$$\tau_{Ref}(\rho_{eff}) = -24.9 \cdot \rho_{eff} + 64.9 \ \text{MPa} \qquad (10)$$

The uniaxial fatigue curve experimentally determined under a load ratio, R, equal to 0.1 was used to estimate both the mean stress sensitivity index and the limiting value for ρ_{eff}, giving m=1 and ρ_{lim}=2.

The error diagram reported in Fig. 9b clearly shows that the MWCM used along with the notch stress concept gives life predictions that generally fall within the two calibration scatter bands, with only a few experimental results being non-conservative (i.e., series δ=90°, $B_R = \sqrt{3}$, R=-1).

Since the reference radius based approach [45] was seen to be capable of modelling the fatigue behaviour of the tested FS welded tubes under both pure axial (Fig. 6e) and pure torsional loading (Fig. 6f), the MWCM was subsequently applied with the undercut groove tip given a fictitious radius, r_f, equal to 0.05 mm [46]. As recommended by Sonsino [33, 46] for conventional "thin and flexible" aluminium welded joints and by Barsoum et al. [34] for aluminium FS welded connections, the MWCM was calibrated using the FAT 160 uniaxial design curve with negative inverse slope equal to 5 (Fig. 6e). The second piece of information used to calibrate the MWCM was the FAT 90 torsional fatigue curve [46] with negative inverse slope equal to 7 [33]. These calibration assumptions used with the MWCM gave the following values for the constants in the governing equations:

$$k_\tau(\rho_{eff}) = -2 \cdot \rho_{eff} + 7 \qquad (11)$$

$$\tau_{Ref}(\rho_{eff}) = -7.2 \cdot \rho_{eff} + 64.8 \ \text{MPa} \tag{12}$$

When designing against fatigue of conventional as-welded joints, the IIW recommends using the design curves provided by disregarding the presence of non-zero mean stresses [32]. Since these FS welded tubes were tested in the as-welded condition, this recommendation was directly incorporated into the MWCM by simply setting the mean stress sensitivity index, m, equal to zero [44]. The R=0 uniaxial fatigue curve recalculated according to the r_f=0.05 mm concept was used to estimate the limiting value for ratio ρ_{eff}, obtaining ρ_{lim}=2.

The error diagram of Fig. 9c clearly demonstrates that the MWCM applied along with the reference radius approach gave lifetime estimates mainly falling within the calibration scatter bands. This result is certainly remarkable, especially in the light of the fact that the calibration process was based on the reference design curves recommended by Sonsino [33, 46] for conventional aluminium welded joints (i.e., determined by considering a different joining technology).

6.4. MWCM applied in conjunction with the Point Method

The Point Method (PM) [66, 67] postulates that the fatigue strength of notched metals can be predicted by using the linear-elastic stress state at a material-dependent distance from the tip of the stress concentration being assessed. By performing a systematic validation exercise based on a large amount of experimental data, it has been demonstrated that the MWCM applied along with the PM can successfully estimate the fatigue strength of notched components subjected to multiaxial fatigue loading, under both constant [68-72] and variable amplitude [73-75] multiaxial load histories. The MWCM used in conjunction with the PM has also been observed to be capable of accurately estimating the fatigue lifetime of conventional welded aluminium joints [56, 59, 64].

The accuracy obtained by applying the notch reference radius concept in conjunction with the design curves recommended by the IIW to be used for conventional aluminium welded connections (see Figs 6e and 6f) suggests that, in these small diameter FS welded tubes, the local stress concentration at the undercut groove prevails over the effects of the joining technology. Accordingly, it is postulated that the MWCM can be applied in conjunction with the PM to estimate the multiaxial fatigue lifetime of FS welded connections by taking the critical distance as being equal to a unifying value of 0.075 mm which is recommended for conventional aluminium weldments [64]. Using this hypothesis for these FS welded tubes, the relevant linear-elastic stress states were then determined numerically at a distance from the crack initiation locations equal to 0.075 mm (Fig. 3d).

The uniaxial and torsional fully-reversed fatigue curves post-processed in accordance with the PM were used to estimate the constants in Eqs (2) and (3). The resulting two curves (together with the corresponding experimental results) are plotted in Fig. 8e in terms of linear-elastic stresses determined at a distance from the undercut tip equal to 0.75 mm (Fig. 3d). The Mohr's circles shown in Fig. 8f indicate that, under fully-reversed nominal uniaxial fatigue loading, the sub-surface tri-axial stress state resulted in a local value of ratio ρ_{eff} equal to 1.185. Under fully-reversed nominal torsional loading, ρ_{eff} was invariably equal to zero (Fig. 8f). The use of the modified Wöhler curves plotted in Fig. 8e gave the following values for the MWCM's calibration constants:

$$k_{\tau}(\rho_{eff}) = -3.7 \cdot \rho_{eff} + 10.8 \tag{13}$$

$$\tau_{Ref}(\rho_{eff}) = -24.8 \cdot \rho_{eff} + 58.0 \tag{14}$$

The uniaxial fatigue curve with R=0.1 re-calculated using the PM (Fig. 3d) was applied to estimate both mean stress sensitivity index m and the limiting value for ratio ρ_{eff}, giving m=1 and ρ_{lim}=1.6.

The experimental life to failure, N_f, versus the estimated number of cycles to failure, $N_{f,e}$, is shown in Fig. 8d and provides a summary of the overall accuracy that was obtained by applying the MWCM in conjunction with the PM. Fig. 9d demonstrates that the systematic use of this linear-elastic local stress based design methodology provides remarkably accurate life estimates, with predictions falling within the scatter bands associated with the experimental calibration fatigue curves.

To conclude, it is worth observing that, compared to the other stress analysis strategies investigated in the previous sections, the MWCM applied in conjunction with the PM can be used also to quantify the detrimental effect of welding defects/imperfections by modelling them explicitly. Further, weld flaws could also be classified according to type, shape, size, position, etc. The criticality level of different families of flaws could then be assessed and quantified by performing parametric numerical studies. The results from these studies would guide and inform the quality assurance process without the need for systematically performing detailed FE stress analyses to model the detrimental effect of standard weld flaws.

7. CONCLUSIONS

- The fatigue behaviour of these small diameter FS welded tubular joints of Al 6082-T6 has been modelled successfully using notch mechanics concepts.

- The MWCM applied in terms of nominal and notch stresses as well as using the PM was seen to be remarkably accurate in providing estimates of the fatigue lifetime of the FS welded joints.

- The MWCM was also seen to be capable of correctly modelling the presence of superimposed static stresses as well as the degree of multiaxiality and non-proportionality of the applied load path.

- Independently of the particular stress analysis strategy adopted, the resulting level of accuracy is certainly satisfactory (see Fig. 9), since, from a statistical point of view, a

predictive method cannot be expected to be more accurate than the experimental information used to calibrate the method itself.

- This paper provides, for the first time, a full analysis of the life prediction techniques that can be successfully applied to the multiaxial fatigue of aluminium tubes joined by friction stir welding. It has clearly shown that the MWCM can be adapted to such components and has opened the way to wider industrial use of friction stir welded tubular space-frame structures.

ACKNOWLEDGMENT

REFERENCES

[1] Stephens RI, Fatemi A, Stephens RR, Fuchs HO. *Metal Fatigue in Engineering*. 2nd Edition, Wiley, New York, USA, 2000.

[2] Reed RP, Smith JH, Christ BW. *The Economic Effects of Fracture in the United States.* U.S. Department of Commerce, National Bureau of Standards, Special Publication 647, March 1983.

[3] Faria L. *The economic effect of fracture in Europe.* Final report of European Atomic Energy Community - Study contract no. 320105, 1991.

[4] Anon. Design of steel structures. ENV 1993-1-1, EUROCODE 3, 1988.

[5] Anon. Design of aluminium structures – Part 2: Structures susceptible to fatigue. ENV 1999, EUROCODE 9, 1999.

[6] Chiteka K. Friction Stir Welding of steels: A Review Paper. IOSR Journal of Mechanical and Civil Engineering, 2013; 9 3:16-20.

[7] Shah S, Tosunoglu S. Friction stir welding: current state of the art and future prospects. In: 16th World Multi-Conference on Systemics, Cybernetics and Informatics, Orlando, Florida, 17-20 July 2012 (available at www.eng.fiu.edu).

[8] Colligan KJ. Friction stir welding for ship construction, Contract N0014-06-D-0048 for the Office of Naval Research, Concurrent Technologies Corporation, Harrisburg, PA, 2004 (available at www.nmc.ctc.com).

[9] Thomas WM, Nicholas ED. Friction stir welding for the transportation industries. Mater Design 1997;18 4/6:269-273.

[10] Burford D, Widener C, Tweedy B. Advances in Friction Stir Welding for Aerospace Applications. In: 6th AIAA Aviation Technology, Integration and operations Conference, American Institute for Aviation and Astronautics, 2006. doi: 10.2514/6.2006-7730.

[11] Anon. American National Standards Institute, AWS D17.3/D17.3M:2010, Specification for friction stir welding of aluminum alloys for aerospace hardware, American Welding Society, 2010.

[12] Anon. MSFC Technical Standard EM 30, MSFC-SPEC-3679, Process specification – welding aerospace hardware, National Space and Aeronautics Administration, October 2012.

[13] Lomolino S, Tovo R, dos Santos J. On the fatigue behaviour and design curves of friction stir butt-welded Al alloys. Int J Fatigue 2005;27 3:305-316.

[14] Maggiolini E, Tovo R, Susmel L, James MN, Hattingh DG. Crack path and fracture analysis in FSW of small diameter 6082-T6 aluminium tubes under tension-torsion loading. Int J Fatigue (2016), http://dx.doi.org/10.1016/j.ijfatigue.2016.02.043.

[15] Moreira PMGP, Santos T, Tavares SMO, Richter-Trummer V, Vilaça P, de Castro PMST. Mechanical and metallurgical characterization of friction stir welding joints of AA6061-T6 with AA6082-T6. Mater Design 2009;30:180-187.

[16] Spindel JE, Haibach E. Some considerations in the statistical determination of the shape of S-N curves. In: Little RE, Ekvall JC. editors. Statistical Analysis of Fatigue Data, ASTM STP 744; 1981. p. 89–113.

[17] Haibach E. Service fatigue-strength – methods and data for structural analysis. VDI, Düsseldorf, Germany, 1992.

[18] Costa JD, Ferreira JAM, Borrego LP. Influence of spectrum loading on fatigue resistance of AA6082 friction stir welds. Int J Struct Integrity 2011;2(2):122–34.

[19] Cavaliere P, Campanile G, Panella F, Squillace A. Effect of welding parameters on mechanical and microstructural properties of AA6056 joints produced by Friction Stir Welding. J Mater Process Technol 2006;180:263-270.

[20] Moreira PMGP, de Figueiredo MAV, de Castro PMST. Fatigue behaviour of FSW and MIG weldments for two aluminium alloys. Theor Appl Fract Mec 2007;48:169–177.

[21] Cavaliere P, Squillace A, Panella F. Effect of welding parameters on mechanical and microstructural properties of AA6082 joints produced by friction stir welding. J Mater Process Technol 2008;200:364–372.

[22] Scialpi A, De Giorgi M, De Filippis LAC, Nobile R, Panella FW. Mechanical analysis of ultra-thin friction stir welding joined sheets with dissimilar and materials. Mater Design 2008;29:928–936.

[23] Cavaliere P, De Santis A, Panella F, Squillace A. Thermoelasticity and CCD analysis of crack propagation in AA6082 friction stir welded joints. Int J Fatigue 2009; 31:385–392.

[24] De Giorgi M, Scialpi A, Panella FW, De Filippis LAC. Effect of shoulder geometry on residual stress and fatigue properties of AA6082 fsw joints. J Mech Sci Technol 2009; 23:26-35.

[25] Cirello A, Buffa G, Fratini L, Pasta S. AA6082-T6 friction stir welded joints fatigue resistance: influence of process parameters. P I Mech Eng B-J Eng 2006;220:805-811.

[26] Krasnowski K, Sedek P, Łomozik M, Pietras A. Impact of selected fsw process parameters on mechanical properties of 6082-t6 aluminium alloy butt joints. Arch Metall Mater 2011;56 4:965-973.

[27] Maddox SJ. Review of fatigue assessment procedures for welded aluminium structures. Int J Fatigue 2003;25:1359–1378.

[28] Ericsson M, Sandstrom, R. Influence of welding speed on the fatigue of friction stir welds, and comparison with MIG and TIG. Int J Fatigue 2003;25:1379–1387.

[29] Costa JD, Ferreira JAM, Borrego LP, Abreu LP. Fatigue behaviour of AA6082 friction stir welds under variable loadings. Int J Fatigue 2012;37:8–16.

[30] Uematsu Y, Tokaji K, Shibata H, Tozaki Y, Ohmune T. Fatigue behaviour of friction stir welds without neither welding flash nor flaw in several aluminium alloys. Int J Fatigue 2009;31:1443–1453.

[31] Sano Y, Masaki K, Gushi T, Sano T. Improvement in fatigue performance of friction stir welded A6061-T6 aluminum alloy by laser peening without coating. Mater Design 2012; 36:809–814.

[32] Hobbacher A. Recommendations for fatigue design of welded joints and components. IIW document XIII-2151-07/XV-1254-07; May 2007.

[33] Sonsino CM, Bruder T, Baumgartner J. SN-curves for welded thin joints – suggested slopes and fat-values for applying the notch stress concept with various reference radii. IIW-Doc. No. XIII-2280 (2009)/XV-1325 (2009); 2009.

[34] Barsoum Z., Khurshid M., Barsoum I. Fatigue strength evaluation of friction stir welded aluminium joints using the nominal and notch stress concepts. Mater Design 2012; 41:231–238.

[35] Prime MB, Gnaupel-Herold T, Baumann JA, Lederich RJ, Bowden DM, Sebring Robert J. Residual stress measurements in a thick, dissimilar aluminum alloy friction stir weld. Acta Mater 2006;54:4013–4021.

[36] Nandan R, DebRoy T, Bhadeshia HKDH. Recent advances in friction-stir welding – Process, weldment structure and properties. Prog Mater Sci 2008;53:980–1023.

[37] Sato YS, Kokawa H, Ikeda K, Enomoto M, Jogan S, Hashimoto T. Microtexture in the Friction-Stir Weld of an Aluminum Alloy. Metall Mater Trans A 2001;32:941-948.

[38] Wert JA. Microstructures of friction stir weld joints between an aluminium-base metal matrix composite and monolithic aluminium alloy. Scripta Mater 2003;49:607–612.

[39] Park SHC, Sato YS, Kokawa H. Basal Plane Texture and Flow Pattern in Friction Stir Weld of a Magnesium Alloy. Metall Mater Trans A 2003;34:987-994.

[40] Thomas WM, Nicholas ED. Friction stir welding for the transportation industries. Mater Design 2997; 18:269-273.

[41] Park SHC, Sato YS, Kokawa H.Effect of micro-texture on fracture location in friction stir weld of Mg alloy AZ61 during tensile test. Scripta Mater 2003;49:161–166.

[42] Sines G. Behaviour of metals under complex static and alternating stresses. In: Sines G, Waisman JL, editors. Metal fatigue. New York: McGraw-Hill; 1959. p. 145–69.

[43] Davoli P, Bernasconi A, Filippini M, Foletti S, Papadopoulos IV. Independence of the torsional fatigue limit upon a mean shear stress. Int J Fatigue 2003;25:471–80.

[44] Susmel L. Multiaxial notch fatigue: from nominal to local stress–strain quantities. Cambridge (UK): Woodhead Publishing Limited; 2009, ISBN 1 84569 582 8.

[45] Radaj D, Sonsino CM, Fricke W. Fatigue assessment of welded joints by local approaches. Cambridge (UK): Woodhead Publishing Limited; 2007.

[46] Sonsino CM. A consideration of allowable equivalent stresses for fatigue design of welded joints according to the notch stress concept with the reference radii r_{ref} = 1.00 and 0.05 mm. Weld World 2009;53(3/4):R64–75.

[47] Susmel L, Lazzarin P. A Bi-Parametric Modified Wöhler Curve for High Cycle Multiaxial Fatigue Assessment. Fatigue Fract Engng Mater Struct 2002;25:63-78.

[48] Lazzarin P, Susmel L. A Stress-Based Method to Predict Lifetime under Multiaxial Fatigue Loadings. Fatigue Fract Engng Mater Struct 2003;26:1171-1187.

[49] Susmel L. Multiaxial Fatigue Limits and Material Sensitivity to Non-Zero Mean Stresses Normal to the Critical Planes. Fatigue Fract Engng Mater Struct 2008;31:295-309.

[50] Susmel L, Tovo R, Lazzarin P. The mean stress effect on the high-cycle fatigue strength from a multiaxial fatigue point of view. Int J Fatigue 2005;27:928-943.

[51] Kaufman RP, Topper T. The influence of static mean stresses applied normal to the maximum shear planes in multiaxial fatigue. In: Biaxial and Multiaxial fatigue and Fracture, Edited by A. Carpinteri, M. de Freitas and A. Spagnoli, Elsevier and ESIS, Oxford, UK, pp. 123-143, 2003.

[52] Susmel L. A simple and efficient numerical algorithm to determine the orientation of the critical plane in multiaxial fatigue problems. Int J Fatigue 2010;32:1875–1883.

[53] Susmel L, Tovo R, Socie DF. Estimating the orientation of Stage I crack paths through the direction of maximum variance of the resolved shear stress. Int J Fatigue 2014;58:94–101.

[54] Susmel L, Tovo R. Estimating Fatigue Damage under Variable Amplitude Multiaxial Fatigue Loading. Fatigue Fract Engng Mater Struct 2011;34:1053-1077.

[55] Susmel L. Three different ways of using the Modified Wöhler Curve Method to perform the multiaxial fatigue assessment of steel and aluminium welded joints. Eng Fail Anal 2009;16:1074–1089.

[56] Susmel L. Four stress analysis strategies to use the Modified Wöhler Curve Method to perform the fatigue assessment of weldments subjected to constant and variable amplitude multiaxial fatigue loading. Int J Fatigue 2014;64:38-54.

[57] Susmel L, Tovo R. On the use of nominal stresses to predict the fatigue strength of welded joints under biaxial cyclic loadings. Fatigue Fract Engng Mater Struct 2004;27:1005-1024.

[58] Susmel L, Tovo R, Benasciutti D. A novel engineering method based on the critical plane concept to estimate the lifetime of weldments subjected to variable amplitude multiaxial fatigue loading. Fatigue Fract Engng Mater Struct 2009;32:441–459.

[59] Susmel L, Askes H. Modified Wöhler Curve Method and multiaxial fatigue assessment of thin welded joints. Int J Fatigue 2012;43:30–42.

[60] Susmel L. Nominal stresses and Modified Wöhler Curve Method to perform the fatigue assessment of uniaxially-loaded inclined welds. P I Mech Eng C-J Mec 2014;228 16:2871-2880.

[61] Susmel L, Tovo R. Local and structural multiaxial stress states in welded joints under fatigue loading. Int J Fatigue 2006;28:564-575.

[62] Susmel L, Sonsino CM, Tovo R. Accuracy of the Modified Wöhler Curve Method applied along with the r_{ref}=1 mm concept in estimating lifetime of welded joints subjected to multiaxial fatigue loading. Int J Fatigue 2011;33:1075-1091.

[63] Susmel L. Modified Wöhler Curve Method, Theory of Critical Distances and EUROCODE 3: a novel engineering procedure to predict the lifetime of steel welded joints subjected to both uniaxial and multiaxial fatigue loading. Int J Fatigue 2008;30:888-907.

[64] Susmel L. The Modified Wöhler Curve Method calibrated by using standard fatigue curves and applied in conjunction with the Theory of Critical Distances to estimate fatigue lifetime of aluminium weldments. Int J Fatigue 2009;31:197-212.

[65] Susmel L. Estimating fatigue lifetime of steel weldments locally damaged by variable amplitude multiaxial stress fields. Int J Fatigue 2010;32:1057–1080.

[66] Peterson RE. Notch Sensitivity. In: Metal Fatigue, Edited by G. Sines and J. L. Waisman, McGraw Hill, New York, 1959, pp. 293-306.

[67] Taylor D. The Theory of Critical Distances: A New Perspective in Fracture Mechanics. Elsevier Science, 2007.

[68] Susmel L, Taylor D. Two methods for predicting the multiaxial fatigue limits of sharp notches. Fatigue Fract Engng Mater Struct 2003;26:821-833.

[69] Susmel L. A unifying approach to estimate the high-cycle fatigue strength of notched components subjected to both uniaxial and multiaxial cyclic loadings. Fatigue Fract Engng Mater Struct 2004;27:391-411.

[70] Susmel L, Taylor D. A simplified approach to apply the theory of critical distances to notched components under torsional fatigue loading. Int J Fatigue 2006;28:417-430.

[71] Susmel L, Taylor D. The Modified Wöhler Curve Method applied along with the Theory of Critical Distances to estimate finite life of notched components subjected to complex multiaxial loading paths. Fatigue Fract Engng Mater Struct 2008;31 12:1047-1064.

[72] Louks R, Gerin B, Draper J, Askes H, Susmel L. On the multiaxial fatigue assessment of complex three-dimensional stress concentrators. Int J Fatigue 2014;63:12-24.

[73] Susmel L, Taylor D. Taking full advantage of nominal stresses to design notched components against variable amplitude multiaxial fatigue. Key Eng Mat 2012;488-489:747-750.

[74] Susmel L, Taylor D. A critical distance/plane method to estimate finite life of notched components under variable amplitude uniaxial/multiaxial fatigue loading. Int J Fatigue 2012;38:7-24.

[75] Susmel L, Taylor D. The Theory of Critical Distances to estimate finite lifetime of notched components subjected to constant and variable amplitude torsional loading. Eng Fract Mech 2013;98:64-79.

List of Captions

Tables

Code	$\sigma_{x,a}$ [MPa]	$\sigma_{x,m}$ [MPa]	$\tau_{xy,a}$ [MPa]	$\tau_{xy,m}$ [MPa]	R	δ [°]	B_R	N_f [Cycles to Failure]
W115	44.1	0.0	0.0	0.0	-1	-	∞	697953
W111	66.2	0.0	0.0	0.0	-1	-	∞	19763
W127	59.5	0.0	0.0	0.0	-1	-	∞	81298
W114	39.7	0.0	0.0	0.0	-1	-	∞	463257
W123	30.9	0.0	0.0	0.0	-1	-	∞	2000000
W116	39.7	0.0	0.0	0.0	-1	-	∞	2000000
W119	66.2	0.0	0.0	0.0	-1	-	∞	17120
W121	39.7	0.0	0.0	0.0	-1	-	∞	476829
W125	35.2	0.0	0.0	0.0	-1	-	∞	2000000
T3	0.0	0.0	33.3	0.0	-1	-	0.0	2000000
T4	0.0	0.0	37.5	0.0	-1	-	0.0	1304324
T5	0.0	0.0	37.5	0.0	-1	-	0.0	1664764
T6	0.0	0.0	41.7	0.0	-1	-	0.0	1726450
T7	0.0	0.0	41.7	0.0	-1	-	0.0	601946
T8	0.0	0.0	50.0	0.0	-1	-	0.0	275020
T9	0.0	0.0	50.0	0.0	-1	-	0.0	155896
T10	0.0	0.0	50.0	0.0	-1	-	0.0	917913
T11	0.0	0.0	66.6	0.0	-1	-	0.0	2053
T12	0.0	0.0	58.3	0.0	-1	-	0.0	31589
T21	0.0	0.0	58.3	0.0	-1	-	0.0	11941
IPh1	47.4	0.0	27.4	0.0	-1	0	$\sqrt{3}$	47641
IPh2	47.4	0.0	27.4	0.0	-1	0	$\sqrt{3}$	139861
IPh3	39.5	0.0	22.8	0.0	-1	0	$\sqrt{3}$	171506
IPh4	39.5	0.0	22.8	0.0	-1	0	$\sqrt{3}$	369237
IPh5	33.0	0.0	19.0	0.0	-1	0	$\sqrt{3}$	355728
IPh6	33.0	0.0	19.0	0.0	-1	0	$\sqrt{3}$	932288
IPh7	33.0	0.0	19.0	0.0	-1	0	$\sqrt{3}$	513782
IPh8	33.0	0.0	19.0	0.0	-1	0	$\sqrt{3}$	623187
IPh9	39.5	0.0	39.5	0.0	-1	0	1.0	160391
IPh10	39.5	0.0	39.5	0.0	-1	0	1.0	47967
IPh11	34.3	0.0	34.3	0.0	-1	0	1.0	358240
IPh12	34.3	0.0	34.3	0.0	-1	0	1.0	533508
IPh13	30.3	0.0	30.3	0.0	-1	0	1.0	592342
IPh14	30.3	0.0	30.3	0.0	-1	0	1.0	650684
IPh15	30.3	0.0	27.4	0.0	-1	0	1.1	148831
OoPh63	39.5	0.0	22.8	0.0	-1	90	$\sqrt{3}$	173954
OoPh64	33.0	0.0	19.0	0.0	-1	90	$\sqrt{3}$	2000000
OoPh65	33.0	0.0	19.0	0.0	-1	90	$\sqrt{3}$	139484
OoPh66	39.5	0.0	22.8	0.0	-1	90	$\sqrt{3}$	44499
OoPh67	33.0	0.0	19.0	0.0	-1	90	$\sqrt{3}$	46086
OoPh68	33.0	0.0	19.0	0.0	-1	90	$\sqrt{3}$	857580
OoPh69	35.6	0.0	20.5	0.0	-1	90	$\sqrt{3}$	686557
OoPh60	39.5	0.0	22.8	0.0	-1	90	$\sqrt{3}$	47459
OoPh61	35.6	0.0	20.5	0.0	-1	90	$\sqrt{3}$	27892
OoPh62	33.0	0.0	19.0	0.0	-1	90	$\sqrt{3}$	218846
OoPh51	34.3	0.0	34.3	0.0	-1	90	1.0	31603
OoPh52	30.3	0.0	30.3	0.0	-1	90	1.0	61384
OoPh53	21.1	0.0	21.1	0.0	-1	90	1.0	2000000
OoPh54	23.7	0.0	23.7	0.0	-1	90	1.0	2000000
OoPh55	27.7	0.0	27.7	0.0	-1	90	1.0	2000000
OoPh56	29.0	0.0	29.0	0.0	-1	90	1.0	2000000
OoPh57	34.3	0.0	34.3	0.0	-1	90	1.0	24628
OoPh58	30.3	0.0	30.3	0.0	-1	90	1.0	29766
OoPh59	27.7	0.0	27.7	0.0	-1	90	1.0	65298

Table 1. Summary of the experimental results generated under R=-1.

Code	σx,a [MPa]	σx,m [MPa]	τxy,a [MPa]	τxy,m [MPa]	R	δ [°]	BR	Nf [Cycles to Failure]
W128	44.1	53.9	0.0	0.0	0.1	-	∞	67970
W122	35.3	43.1	0.0	0.0	0.1	-	∞	96400
W124	26.5	32.3	0.0	0.0	0.1	-	∞	466154
W120	24.3	29.7	0.0	0.0	0.1	-	∞	1167540
W112	22.1	27.0	0.0	0.0	0.1	-	∞	2000000
W129	44.1	53.9	0.0	0.0	0.1	-	∞	37991
W130	24.3	29.7	0.0	0.0	0.1	-	∞	222671
W117	24.3	29.7	0.0	0.0	0.1	-	∞	709775
W118	22.1	27.0	0.0	0.0	0.1	-	∞	1247627
W113	24.3	29.7	0.0	0.0	0.1	-	∞	2000000
T13	0.0	0.0	41.7	41.7	0	-	0.0	318930
T14	0.0	0.0	41.7	41.7	0	-	0.0	347127
T15	0.0	0.0	37.5	37.5	0	-	0.0	427865
T16	0.0	0.0	33.3	33.3	0	-	0.0	1071840
T17	0.0	0.0	50.0	50.0	0	-	0.0	8764
T18	0.0	0.0	50.0	50.0	0	-	0.0	24610
T19	0.0	0.0	37.5	37.5	0	-	0.0	522030
T20	0.0	0.0	33.3	33.3	0	-	0.0	2000000
T23	0.0	0.0	45.8	45.8	0	-	0.0	208575
T24	0.0	0.0	45.8	45.8	0	-	0.0	275002
IPh-16	33.0	33.0	19.0	19.0	0	0	√3	205952
IPh-17	30.3	30.3	17.5	17.5	0	0	√3	118631
Iph-18	18.5	18.5	10.6	10.6	0	0	√3	2000000
IPh-19	47.4	47.4	27.4	27.4	0	0	√3	25614
IPh-20	23.7	23.7	13.7	13.7	0	0	√3	501988
IPh-21	21.1	21.1	12.2	12.2	0	0	√3	891341
IPh-22	23.7	23.7	13.7	13.7	0	0	√3	2000000
IPh-30	30.3	30.3	30.3	30.3	0	0	1.0	236518
IPh-31	25.0	25.0	25.0	25.0	0	0	1.0	175164
IPh-32	25.0	25.0	25.0	25.0	0	0	1.0	170009
IPh-33	21.1	21.1	21.1	21.1	0	0	1.0	273482
IPh-34	18.5	18.5	18.5	18.5	0	0	1.0	857370
IPh-35	18.5	18.5	18.5	18.5	0	0	1.0	548537
IPh-36	15.8	15.8	15.8	15.8	0	0	1.0	1351096
OoPh-37	33.0	33.0	19.0	19.0	0	90	√3	98938
OoPh-38	29.0	29.0	16.7	16.7	0	90	√3	224230
OoPh-39	23.7	23.7	13.7	13.7	0	90	√3	2000000
OoPh-40	33.0	33.0	19.0	19.0	0	90	√3	38084
OoPh-41	29.0	29.0	16.7	16.7	0	90	√3	121400
OoPh-42	23.7	23.7	13.7	13.7	0	90	√3	2000000
OoPh-43	26.4	26.4	15.2	15.2	0	90	√3	745539
OoPh-44	29.0	29.0	29.0	29.0	0	90	1.0	34544
OoPh-45	21.1	21.1	21.1	21.1	0	90	1.0	2000000
OoPh-46	26.4	26.4	26.4	26.4	0	90	1.0	80612
OoPh-47	25.0	25.0	25.0	25.0	0	90	1.0	945586
OoPh-48	26.4	26.4	26.4	26.4	0	90	1.0	61539
OoPh-49	23.7	23.7	23.7	23.7	0	90	1.0	1089502
OoPh-50	29.0	29.0	29.0	29.0	0	90	1.0	82314

Table 2. Summary of the experimental results generated under R=0÷0.1.

B_R	R	δ [°]	N. of data	k	σ_A[a] [MPa]	τ_A[a] [MPa]	T_σ
∞	-1	-	9	6.5	33.5	-	1.58
∞	0.1	-	10	4.4	18.6	-	1.82
0	-1	-	11	10.8	-	38.9	1.49
0	0	-	10	9.5	-	32.9	1.52
$\sqrt{3}$	-1	0	8	5.3	26.1	15.1	1.55
$\sqrt{3}$	0	0	7	4.2	17.2	9.9	1.73
$\sqrt{3}$	-1	90	10	5.3	21.1	12.2	2.97
$\sqrt{3}$	0	90	7	10.4	23.4	13.5	1.38
1	-1	0	7	5.4	23.2	23.2	2.12
1	0	0	7	3.2	12.8	12.8	2.00
1	-1	90	9	3.9	11.3	11.3	1.66
1	0	90	7	15.8	22.6	22.6	1.35

[a]Endurance limits extrapolated at $N_{Ref}=2\cdot10^6$ cycles to failure.

Table 3. Wöhler fatigue curves determined in terms of nominal stresses referred to the annular section of the parent tube.
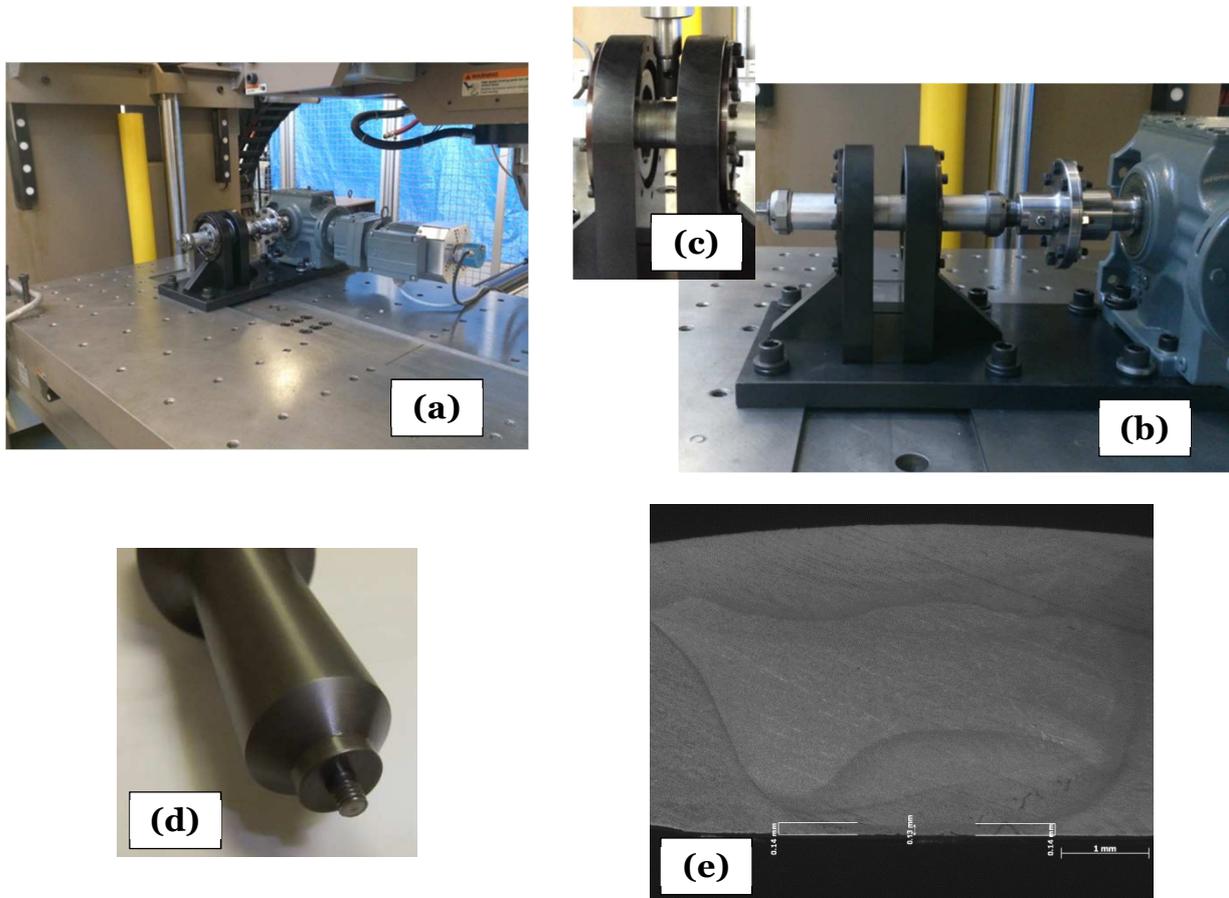
Figure 1. I-STIR FS welding platform equipped with a fourth axis (a); bearing supports with integrated clamping devices (b, c); welding tool developed to circumferentially FS weld tubes (d); example of transverse macro-section of the weld region (e).
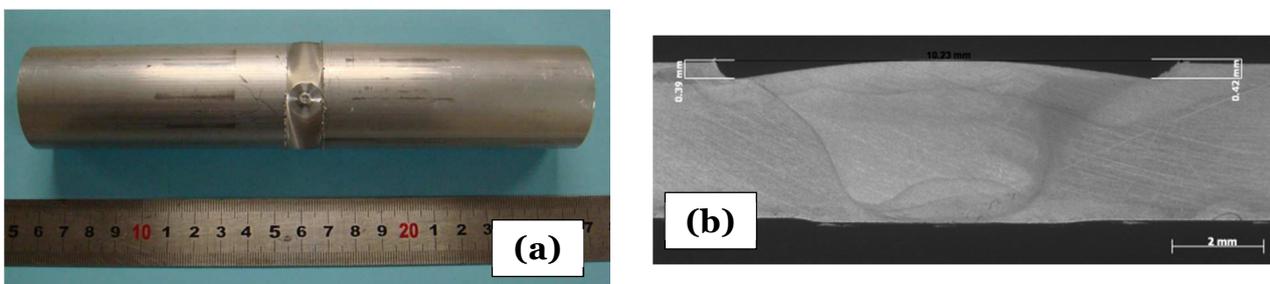
Figure 2. Al 6082-T6 FS welded tubular specimen (a); transverse macro-section of the weld region showing the notches resulting from the joining process (b).
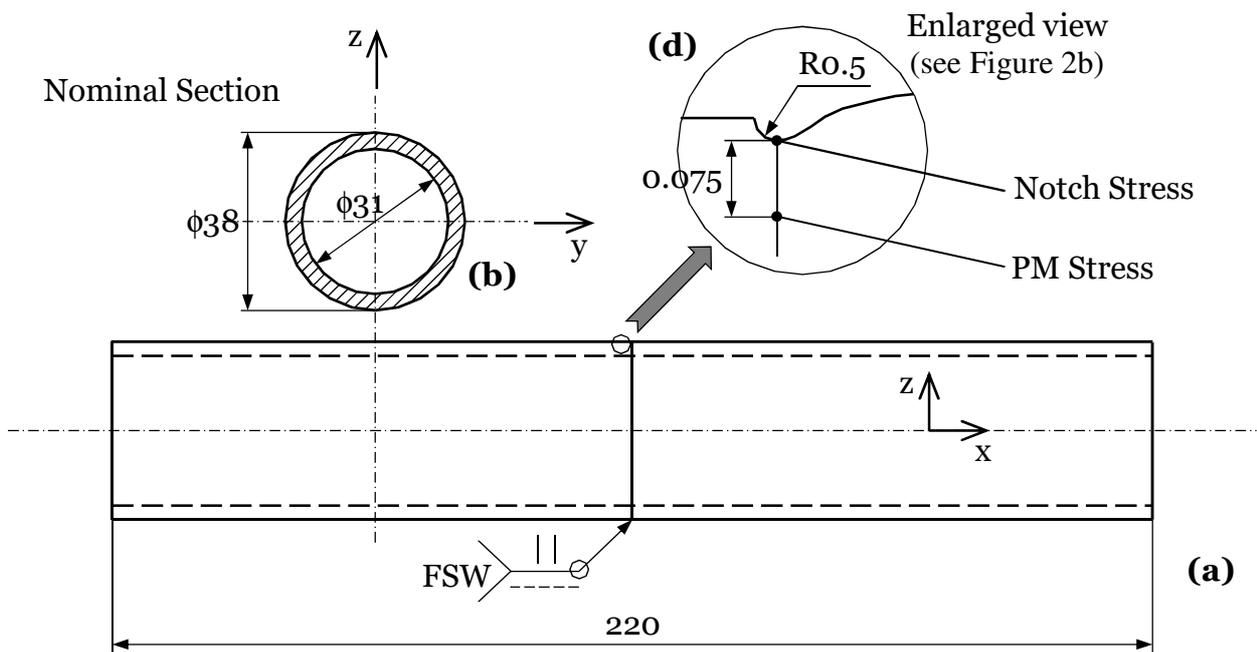
Figure 3. Technical drawing of the FS welded tubular specimen and adopted system of coordinates (dimensions in millimetres).
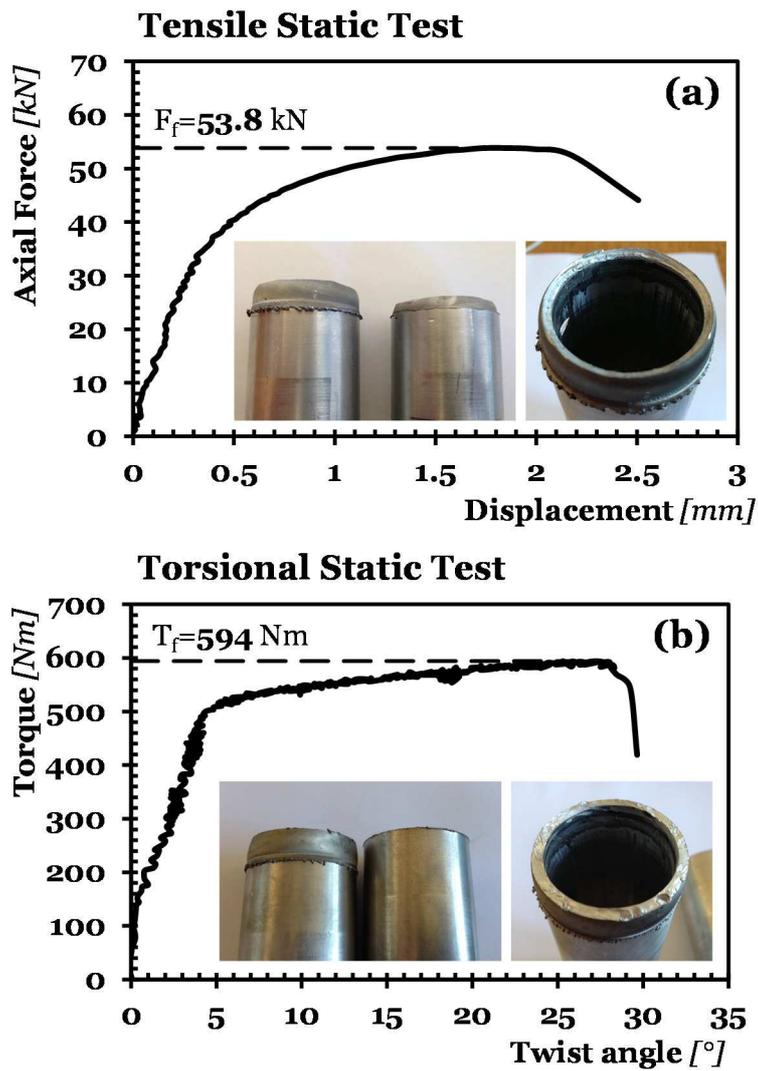
Figure 4. FS welded tubular specimens tested under axial (a) and torsional (b) static loading.

$B_R=0$, R=-1	$B_R=\sqrt{3}$, R=-1, δ=0°	$B_R=1$, R=-1, δ=0°	$B_R=\sqrt{3}$, R=-1, δ=90°	$B_R=1$, R=-1, δ=90°
$B_R=0$, R=-1	$B_R=\sqrt{3}$, R=-1, δ=0°	$B_R=1$, R=-1, δ=0°	$B_R=\sqrt{3}$, R=-1, δ=90°	$B_R=1$, R=-1, δ=90°
$B_R=0$, R=0	$B_R=\sqrt{3}$, R=0, δ=0°	$B_R=1$, R=0, δ=0°	$B_R=\sqrt{3}$, R=0, δ=90°	$B_R=1$, R=0, δ=90°
$B_R=0$, R=0	$B_R=\sqrt{3}$, R=0, δ=0°	$B_R=1$, R=0, δ=0°	$B_R=\sqrt{3}$, R=0, δ=90°	$B_R=1$, R=0, δ=90°
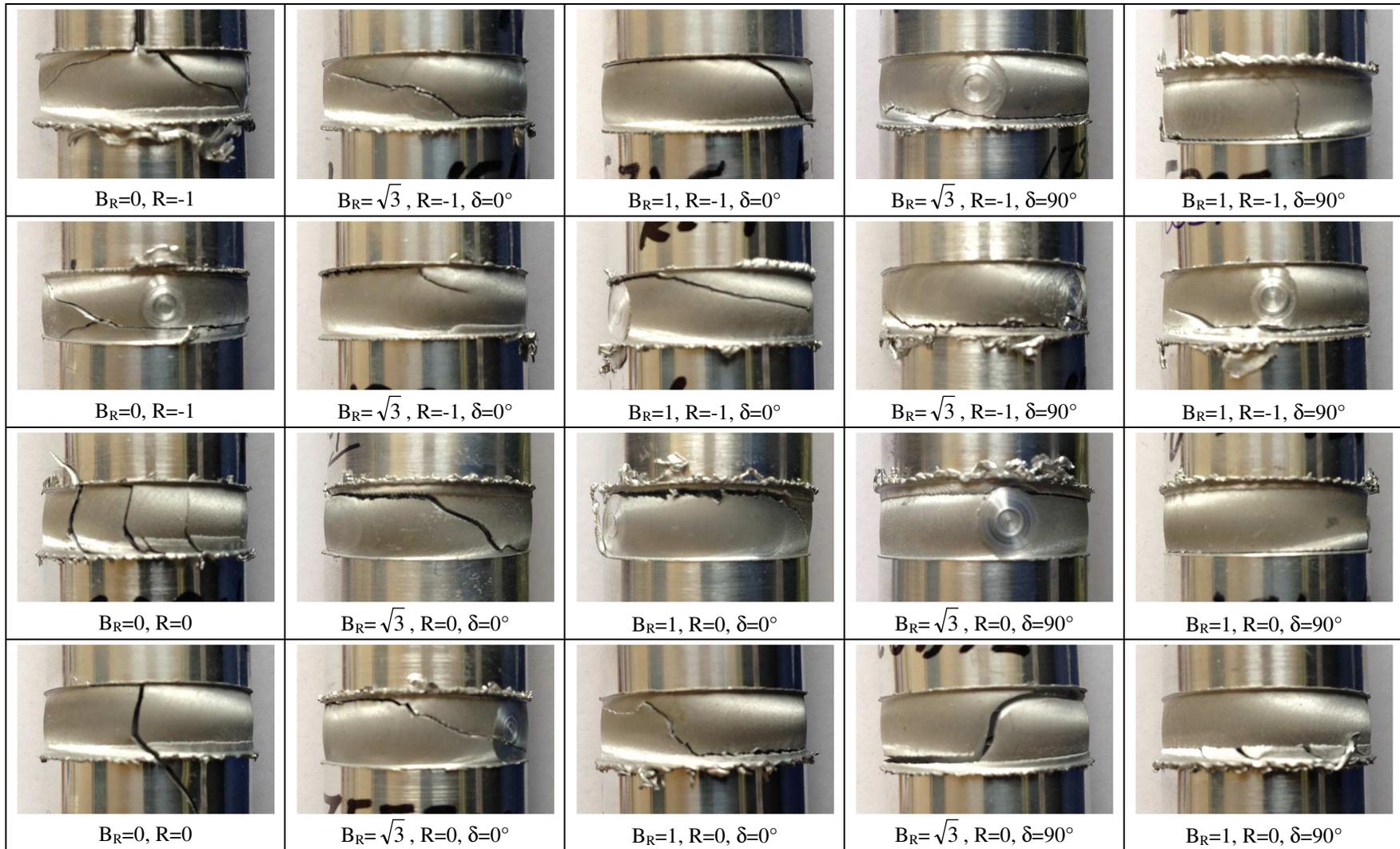
Figure 5. Examples of macroscopic cracking behaviour under biaxial cyclic loading.
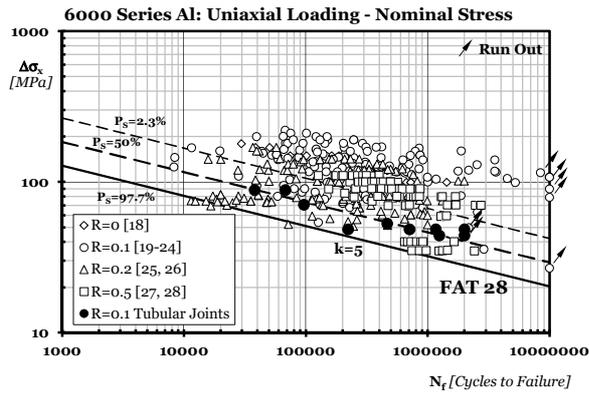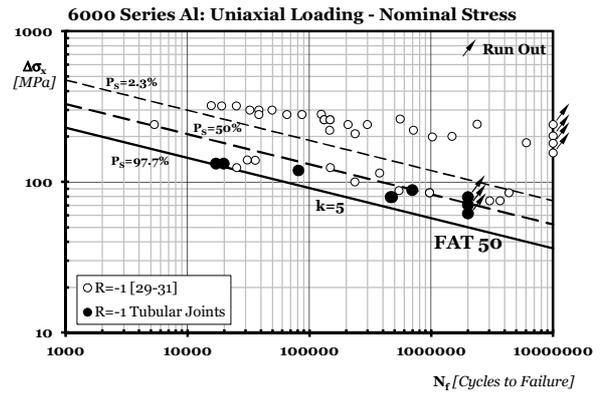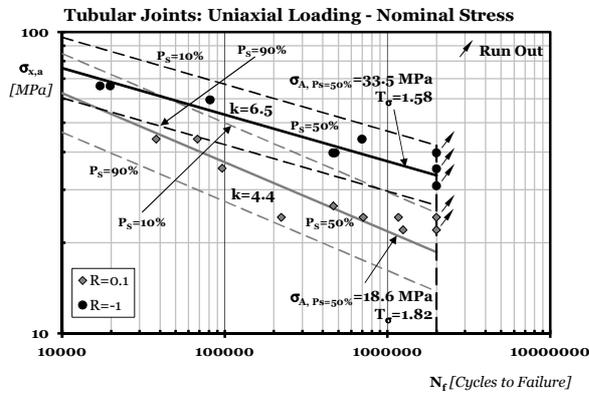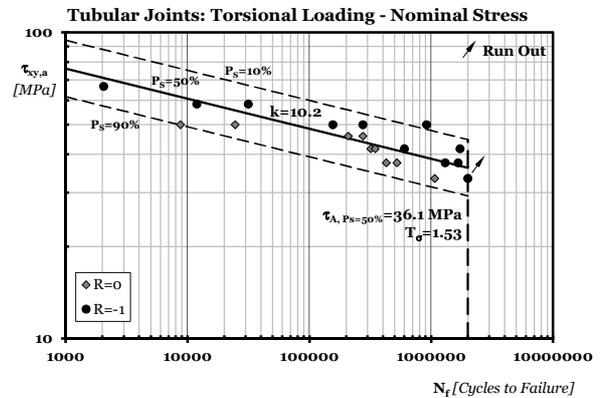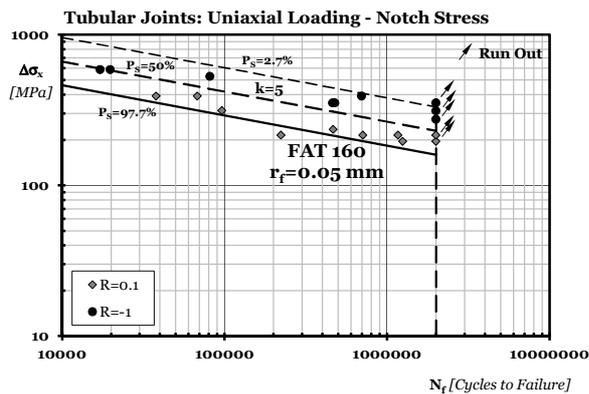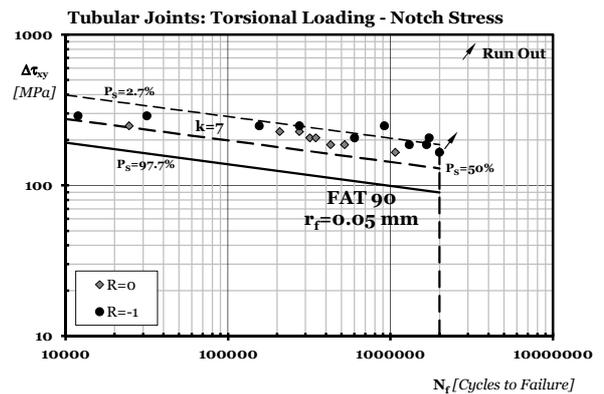
Figure 6. Fatigue strength of the FS welded tubular joints under pure axial
and pure torsional loading.

(a)

(b)
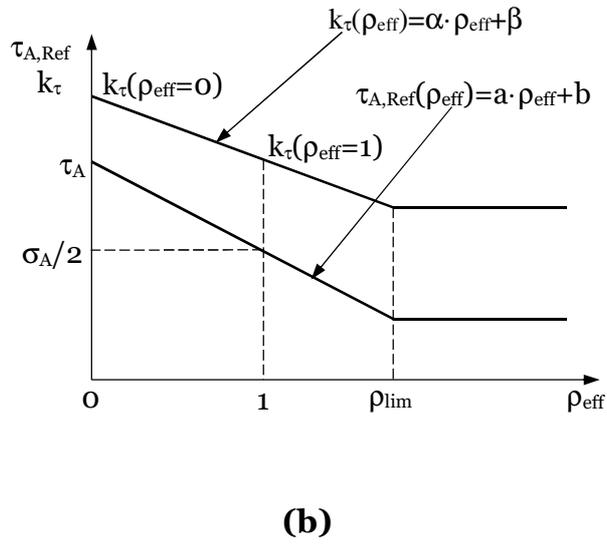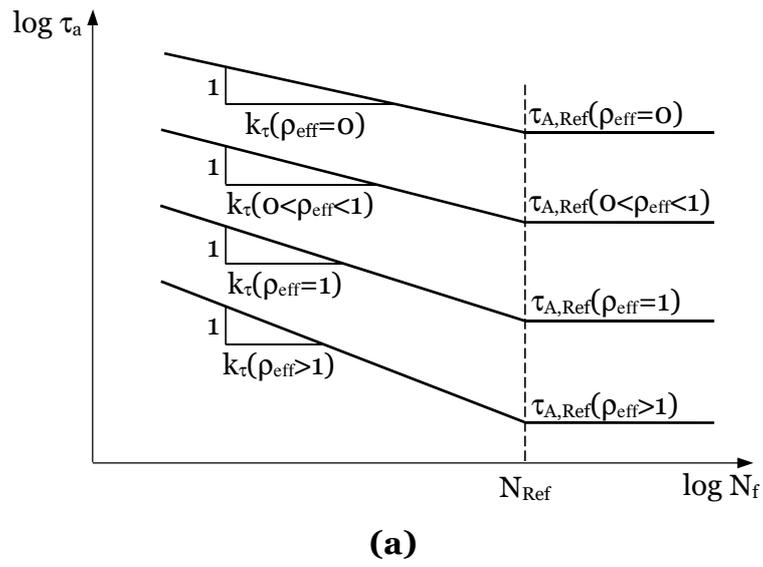
Figure 7. Modified Wöhler diagram (a); MWCM's governing equations (b).
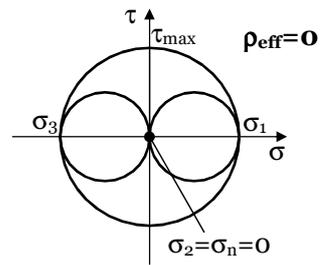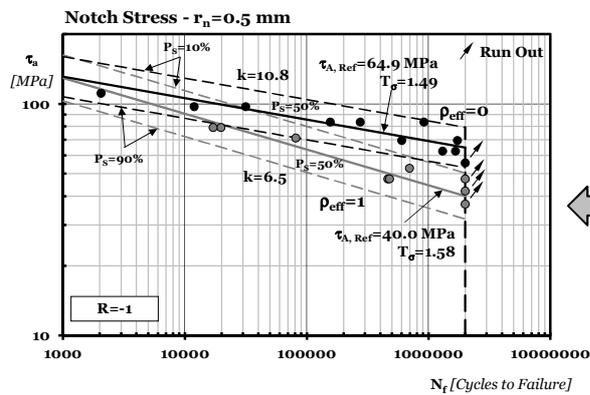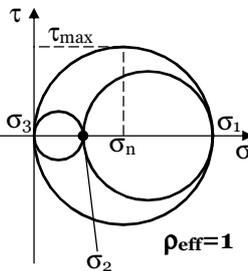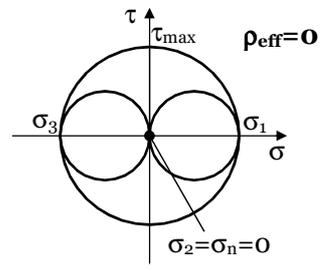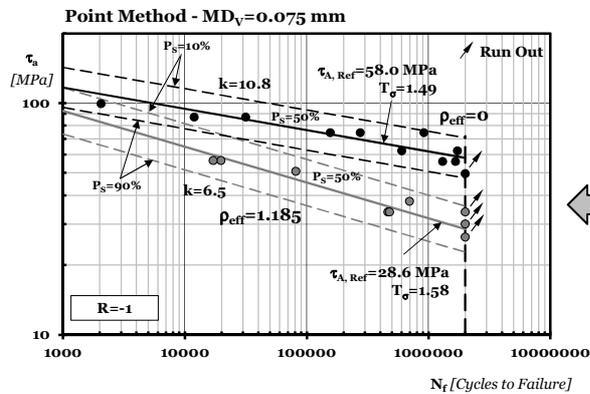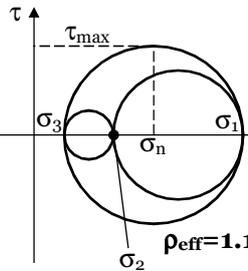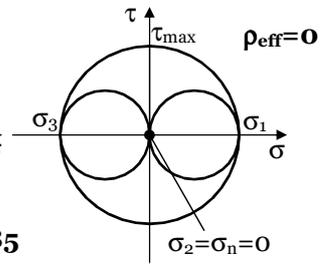
Figure 8. Calibration fatigue curves determined in terms of nominal stresses (a, b) as well as according to the notch stress concept (c, d) and the Point Method (e, f).
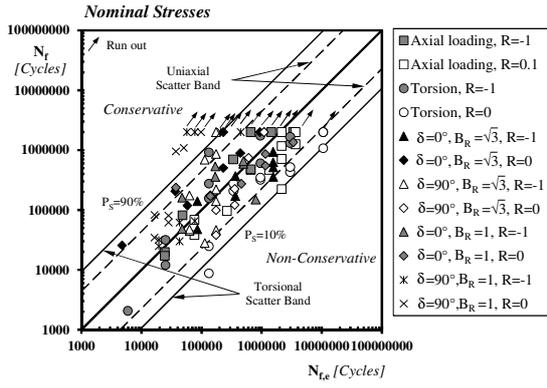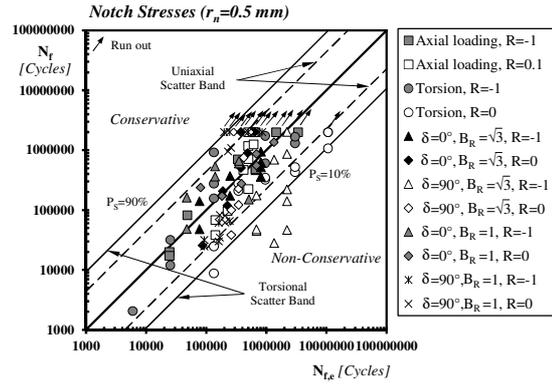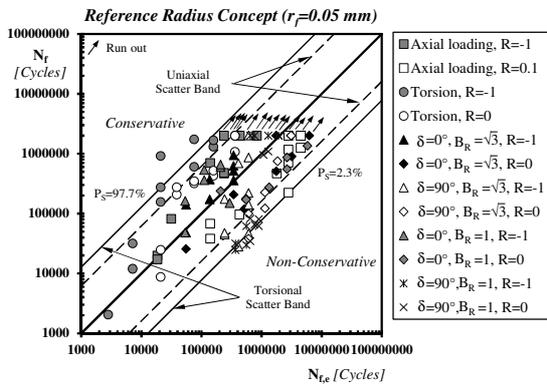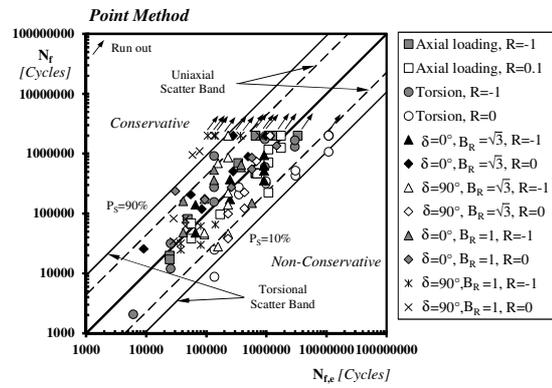
Figure 9. Accuracy of the MWCM in estimating the fatigue lifetime of the tested FS welded tubular joints of Al 6082-T6.